

Intertwined superconductivity and orbital selectivity in a three-orbital Hubbard model for the iron pnictides

Vito Marino,¹ Alberto Scazzola,² Federico Becca,³ Massimo Capone,⁴ and Luca F. Tocchio¹

¹*Institute for Condensed Matter Physics and Complex Systems,
DISAT, Politecnico di Torino, I-10129 Torino, Italy*

²*Department of Electronics and Telecommunications, Politecnico di Torino, I-10129 Torino, Italy*

³*Dipartimento di Fisica, Università di Trieste, Strada Costiera 11, I-34151 Trieste, Italy*

⁴*International School for Advanced Studies (SISSA) and CNR-IOM, Via Bonomea 265, I-34136 Trieste, Italy*
(Dated: June 21, 2024)

We study a three-orbital Hubbard-Kanamori model relevant for iron-based superconductors using variational wave functions, which explicitly include spatial correlations and electron pairing. We span the nonmagnetic sector ranging from a filling $n = 4$, which is representative of undoped iron-based superconductors, to $n = 3$. In the latter case, a Mott insulating state is found, with each orbital at half filling. In the strong-coupling regime, when the electron density is increased, we find a spontaneous differentiation between the occupation of d_{xz} and d_{yz} orbitals, which leads to an orbital-selective state with a nematic character that becomes stronger at increasing density. One of these orbitals stays half filled for all densities while the other one hosts (together with the d_{xy} orbital) the excess of electron density. Most importantly, in this regime long-range pairing correlations appear in the orbital with the largest occupation. Our results highlight a strong link between orbital-selective correlations, nematicity, and superconductivity, which requires the presence of a significant Hund's coupling.

Introduction. The discovery of iron-based superconductors (IBS) [1] enriched the landscape of unconventional superconductivity and tempted the community to compare them with copper-based high- T_c superconductors (cuprates). In both families, superconductivity emerges in rich phase diagrams and competes with quantum phases driven by electron-electron interactions, including spin-density waves and nematic metallic states.

An undisputed difference is the fact that in IBS the low-energy electronic structure features more than one band, calling for the inclusion of different atomic orbitals in the modeling, while copper-based materials are well described in a single-band picture. This entails important consequences for the degree and the nature of electronic correlation in these materials [2]. Indeed, conflicting evidences led to a persistent debate as to whether a weak- or a strong-coupling description is more appropriate [3–9]. In particular, a picture in terms of renormalized itinerant electrons coupled by bosonic excitations, typically of magnetic origin, accounts for several features of the superconducting phase and its interplay with nematic ordering [10–15]. On the other hand, the presence of a sizeable Hund's coupling has been identified as the underlying principle that leads to anomalies of the normal state (leading to the so-called Hund's metal) [3, 16, 17] among which a pivotal role is played by orbital-selective correlations [18], i.e., by the simultaneous presence of strongly correlated and weakly correlated electrons associated with different atomic orbitals. An orbital-selective character has been also reported experimentally both for superconductivity [19] and the normal state [20–22]. Indeed, the Hund's metal has been shown to favor an enhancement (or even a divergence) of the

charge compressibility [23–25] and to favor both superconductivity [26, 27] and nematic ordering [28].

In this scenario, where seemingly contradictory approaches have been successfully used, several fundamental questions remain open. A particularly important and challenging problem is to understand whether superconductivity requires the explicit inclusion of a boson mediating pairing, or whether superconductivity arises directly within the intermediate/strong coupling regime of the local interactions. In Ref. [27], a simplified approach to superconductivity in Hund's metals (inspired by Ref. [29, 30]) has been implemented, showing that a boson-mediated pairing is compatible with a Hund's metal which in turn introduces orbital-selective features. This question is very elusive also for technical reasons. In fact, it is very hard to find a methodology able to simultaneously capture the effects of strong correlations and the low-energy bosonic mediators for the multi-orbital models which are necessary to properly study these materials. Most of the information about the role of Hund's correlations comes from Dynamical Mean-Field Theory (DMFT) [31], which introduces accurate dynamical local correlations, or simpler methods sharing the local focus such as slave particles [32]. However, all these methods do not include non-local correlations beyond static mean-field.

In this work, we make a further step forward by using variational Monte Carlo (VMC) method to investigate the three-orbital Hubbard-Kanamori model [17, 33] used in Ref. [27, 28] and adapted from Ref. [34, 35]. The VMC method allows us to accurately describe non-local correlations and ordering, including non-local superconductivity, none of which is accessible within DMFT. Still,

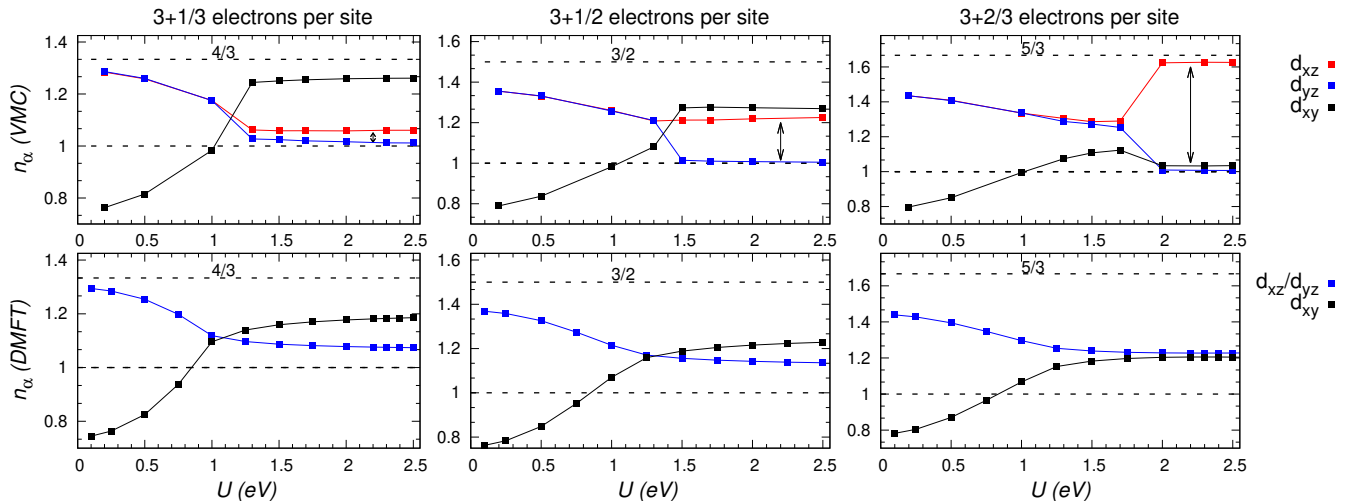


FIG. 1. Upper panels: Electronic density per orbital n_α as a function of U , as obtained within the VMC method for three different total electronic densities: $n = 3 + 1/3$ (left column), $n = 3 + 1/2$ (middle column), and $n = 3 + 2/3$ (right column). We fix $J/U = 0.2$. Data are shown for the $L = 12 \times 12$ cluster. The arrows highlight the size of the differentiation between the d_{xz} and the d_{yz} orbitals. Lower panels: The same as in the upper panels, computed with DMFT and an exact-diagonalization solver.

we work within the nonmagnetic sector, to emphasize the intrinsic correlation effects driven by the Hund's coupling and to establish their relation with superconductivity and orbital symmetric breaking. We follow the evolution of the system as a function of the filling from $n = 4$ which corresponds, in our three-orbital model, to the undoped compounds (which have a filling of 6 electrons in 5 orbitals) to $n = 3$, where a Mott insulator is found.

We observe a ubiquitous spontaneous breaking of the orbital degeneracy between d_{xz} and d_{yz} orbitals which takes place moving away from $n = 3$, where every orbital is half filled. Such a differentiation implies a nematic order in the metallic state. For large electron-electron repulsion, one of the two orbitals remains half filled in the whole density window, while the other becomes more and more filled as we approach $n = 4$, suggesting an orbital-selective Mott transition [36]. Most importantly, the orbital with the largest occupation has sizable pairing correlations, that in a doping range close to $n = 3$ have similarities with the s^\pm structure [4, 37, 38]. We underline that Hund's coupling is necessary to drive both orbital selectivity and superconductivity.

Model and Method. We consider the three-orbital (d_{xz} , d_{yz} , and d_{xy}) Hamiltonian \mathcal{H}_0 [27, 28] that reproduces qualitatively the generic shape and the orbital content of the Fermi surfaces of IBS: Two hole-like pockets around the Γ point and two elliptic electron-like pockets centered at the symmetry-related points X and Y . The explicit form of the Hamiltonian is reported in the Supplemental Material [39]. Importantly, the degeneracy of the three

orbitals is partially lifted by the crystal field (penalizing the d_{xy} orbital over the d_{yz} and d_{zx} , which remain degenerate). As in previous work, we include local Hubbard and Hund's couplings [17, 33]. We underline that our model is not chosen to reproduce detailed features of any individual IBS, but rather as a simplified tight-binding picture, which is sufficiently light to allow for an accurate numerical solution, while containing the main features of the IBS fermiology. For this reason, we will not attempt a direct comparison with experiments, but we will rather extract information about the general trends arising from the interplay between non-local electronic correlations and a sensible electronic structure.

The VMC approach is based on the definition of correlated variational wave functions, whose parameters and properties can be evaluated within a Monte Carlo scheme [40]. In particular, the electron-electron correlation is inserted by Jastrow factors [41, 42] on top of an uncorrelated Bardeen-Cooper-Schrieffer (BCS) state, which is appropriate to describe superconductivity:

$$|\Psi\rangle = \mathcal{J}_c \mathcal{J}_s |\Phi_0\rangle. \quad (1)$$

Here, \mathcal{J}_c and \mathcal{J}_s are density and spin Jastrow factors that are suitable to include correlations within the variational state $\mathcal{J}_c = \exp\left(-\frac{1}{2} \sum_{\alpha,\beta} \sum_{R,R'} v_{R,R'}^{\alpha,\beta} n_{R,\alpha} n_{R',\beta}\right)$ and $\mathcal{J}_s = \exp\left(-\frac{1}{2} \sum_{\alpha \neq \beta} \sum_R u_R^{\alpha,\beta} S_{R,\alpha}^z S_{R,\beta}^z\right)$ where $n_{R,\alpha} = n_{R,\alpha,\uparrow} + n_{R,\alpha,\downarrow}$ and $S_{i,\alpha}^z = (n_{R,\alpha,\uparrow} - n_{R,\alpha,\downarrow})/2$ are the total density and spin along the z axis on site R and orbital α , i.e., $n_{R,\alpha,\sigma} = c_{R,\alpha,\sigma}^\dagger c_{R,\alpha,\sigma}$ (where $c_{R,\alpha,\sigma}^\dagger$ and $c_{R,\alpha,\sigma}$ are

creation and annihilation operators for fermions on site R , orbital α , and spin σ). The parameters $v_{R,R'}^{\alpha,\beta}$ and $u_R^{\alpha,\beta}$ are pseudo-potentials to be optimized to minimize the variational energy [40, 43]. Notice that the density Jastrow factor includes long-range terms, which are important to describe the Mott insulator [41, 42], while the spin-spin ones are limited to on-site terms, in order to include the Hund's effect. The uncorrelated state $|\psi_0\rangle$ is the ground state of an auxiliary Hamiltonian featuring a BCS intra-orbital pairing, in addition to \mathcal{H}_0 :

$$\mathcal{H}_{BCS} = \mathcal{H}_0 - \sum_{R,\alpha,\sigma} \mu_\alpha c_{R,\alpha,\sigma}^\dagger c_{R,\alpha,\sigma} + \sum_{R,\alpha,\delta} \left(\Delta_{\alpha,\delta} c_{R,\alpha,\downarrow} c_{R+\delta,\alpha,\uparrow} + \text{h.c.} \right), \quad (2)$$

where $\delta = x, y, x+y$, and $x-y$ indicates nearest and next-nearest neighbors of the site R and μ_α defines the chemical potential of orbital α . The pairing amplitudes $\Delta_{\alpha,\delta}$ and μ_α are also optimized, while the hopping parameters in \mathcal{H}_0 are kept fixed to the bare Hamiltonian. Inter-orbital pairing amplitudes are found to be negligible in the optimal wave function, in agreement with [44]. Calculations are done on $L = l \times l$ clusters, with periodic boundary conditions, mainly with $l = 12$.

Results. We start with the emergence of the orbital selectivity. In Fig. 1, we report the density occupation of the orbitals $\{n_{xz}, n_{yz}, n_{xy}\}$ for a few representative densities $n = 3 + \delta n$ (with $\delta n = 2/3, 1/2$, and $1/3$) and different values of the Hubbard- U interaction with $J/U = 0.2$. The results are compared with DMFT using an exact-diagonalization solver [45]. For all the cases (including others not shown), the results exhibit the same behavior for small values of the interaction strength U : the two orbitals d_{xz} and d_{yz} have the same electron occupation, which is larger than the one of the orbital d_{xy} (penalized by the crystal field). By increasing U , the difference among the orbitals reduces, since the interaction terms affect all of them in the same way. This initial trend is also found in DMFT. For even larger values of U , the VMC results change drastically. Indeed, for $0 < \delta n \lesssim 0.5$, the d_{xy} orbital (which has sizable intra-orbital hoppings) becomes the most occupied one, while the other ones have smaller occupations, with one of them (e.g., d_{yz}) being half filled and the other one (d_{xz}) having an intermediate occupation, i.e., $n_{xy} > n_{xz} > n_{yz} \approx 1$. This fact implies a nematic feature, which increases moving away from $n = 3$, where no sign of orbital selectivity has been detected. For δn slightly larger than $1/2$, the occupations of d_{xz} and d_{xy} orbitals cross each other. By further increasing δn , n_{xy} tends rapidly to half filling ($n_{xy} \rightarrow 1$), while most of the excess electron density goes into the d_{xz} one ($n_{xz} \approx 1 + \delta n$). We remark that the differentiation between d_{xz} and d_{yz} orbitals is not obtained within the DMFT approach (which, however, predicts the orbital occupation switch), suggesting that it is

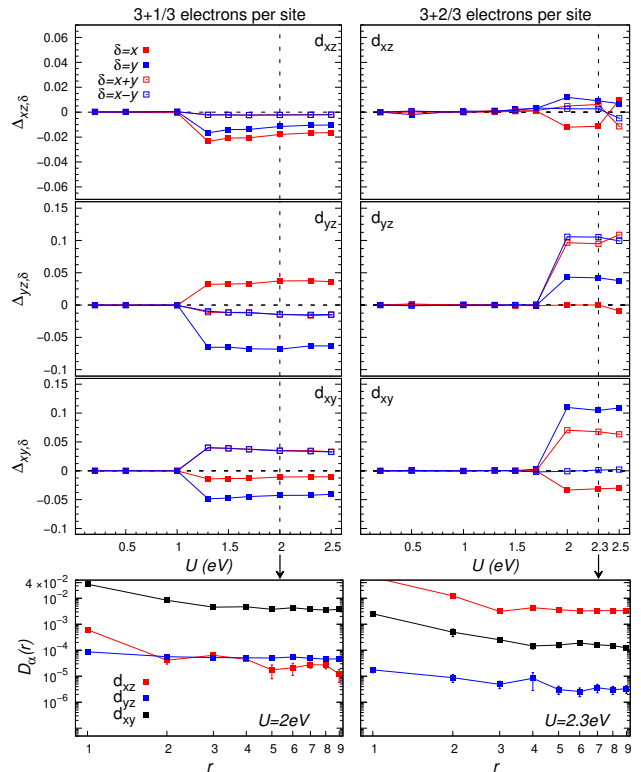


FIG. 2. Upper six panels: Optimal intra-orbital BCS parameters [see Eq. (2)] as a function of U . Lower panels: Pairing correlation function $D_\alpha(r)$ in all orbitals, for a value of U within the orbital-selective regime. Data are shown at total electronic densities $n = 3 + 1/3$ (left column) and $n = 3 + 2/3$ (right column). BCS parameters are computed with the variational approach on a $L = 12 \times 12$ lattice, while the pairing correlations are obtained on a $L = 18 \times 18$ cluster. In all cases $J/U = 0.2$.

driven by (long-range) spatial correlations. This observation is corroborated by the fact that we do not detect any density disproportion between d_{xz} and d_{yz} orbitals when the density-density Jastrow factor is restricted to short-range distances.

Now, we turn to the main result of this work, namely the possible emergence of superconductivity. Within the VMC approach, the presence of superconductivity is usually associated with the stabilization of BCS parameters in the optimized wave function, see Eq. (2) that defines the uncorrelated state $|\psi_0\rangle$. Still, pairing in the uncorrelated part of the wave function does not imply superconducting order, since the Jastrow factor may suppress the actual pairing correlations (e.g., in the Mott regime [41, 42]). Then, in order to assess the true presence of a superconducting state, we compute the intra-orbital pairing correlations $D_\alpha(r) = \frac{1}{L} \sum_R \langle P_{R,\alpha} P_{R+r,\alpha}^\dagger \rangle$ where $P_{R,\alpha} = c_{R+y,\alpha,\downarrow} c_{R,\alpha,\uparrow} - c_{R+y,\alpha,\uparrow} c_{R,\alpha,\downarrow}$ destroys two electrons on the same orbital at nearest-neighbor sites (along

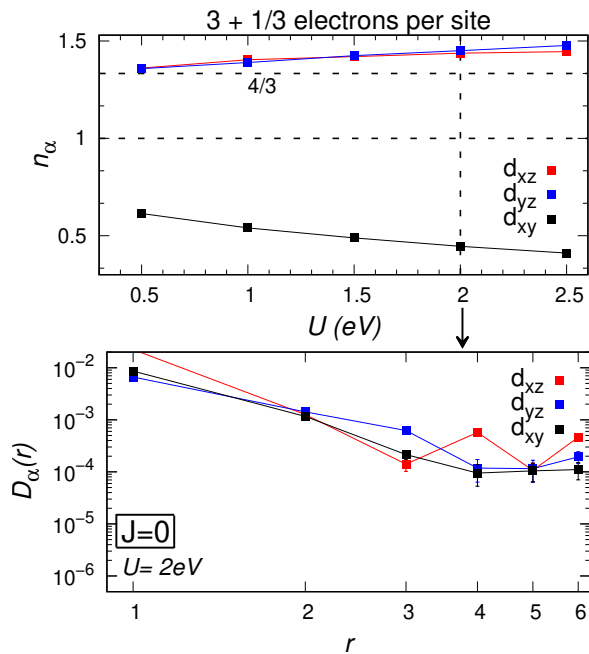


FIG. 3. Electronic density per orbital n_α , as a function of U (upper panel) and pairing correlations $D_\alpha(r)$ for $U = 2\text{eV}$ (lower panel), in the absence of Hund's coupling at density $n = 3 + 1/3$. Data are obtained on a $L = 12 \times 12$ cluster.

y). Then, superconductivity exists whenever $D_\alpha(r)$ does not decay to zero at large distances.

Let us start by considering the optimal (intra-orbital) BCS parameters $\Delta_{\alpha,\delta}$ of Eq. (2). The results for $n = 3 + 2/3$ and $n = 3 + 1/3$ are shown in Fig. 2. In both cases, at sufficiently large values of the Hubbard- U interaction, the orbital selective phase is accompanied by the development of sizable BCS parameters in both d_{xy} and d_{yz} orbitals, while they are relatively small in the d_{xz} one. However, the presence of inter-band hoppings in the Hamiltonian induces a remarkable difference in the pairing correlations: For $n = 3 + 1/3$, the stabilization of finite BCS parameters in the d_{xy} orbital leads to a true superconducting (long-range) correlation $D_{xy}(r)$, see Fig. 2 (for $U = 2\text{eV}$). Instead, the other two orbitals, whose densities are close to half-filling, show a very small signal (in this case, the Jastrow factor gives a substantial suppression of pairing correlations). If we Fourier transform the pairing amplitudes $\Delta_{xy,\delta}$ to k -space in the nematic regime, we find that $\Delta_{xy,k}$ changes sign between the hole pocket around $\Gamma = (0, 0)$ and the electron pockets around the $X = (\pi, 0)$ and $Y = (0, \pi)$, resembling the s^\pm symmetry. However, the underlying nematicity induces a strong difference between X and Y points [39]. The situation is different for $n = 3 + 2/3$, where $n_{xy} \approx 1$ and the pairing correlations $D_{xy}(r)$ are much reduced (again by the Jastrow factor) with respect to the previ-

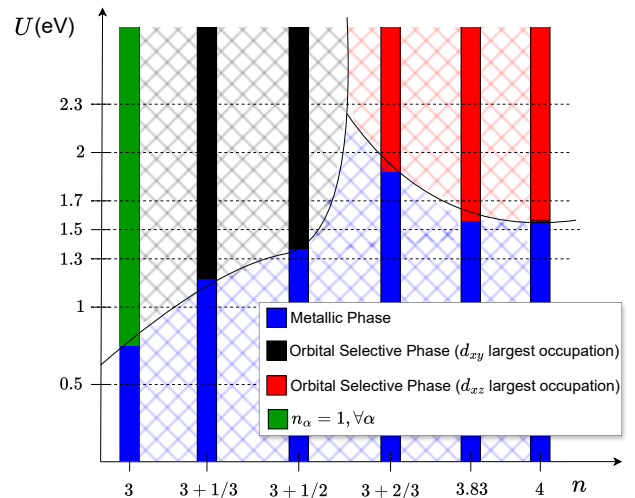


FIG. 4. Ground-state phase diagram of the three-orbital model, as reconstructed from the calculations on selected electron densities. The Hund's coupling is fixed to $J/U = 0.2$. The red and the black regions are characterized by the development of superconductivity, as discussed in the text.

ous case, see Fig. 2 ($U = 2.3\text{eV}$). However, surprisingly, the d_{xz} orbital (which is not half-filled) shows sizable pairing correlations, despite having relatively small BCS parameters. This fact is only possible because of the inter-orbital hybridization in the BCS Hamiltonian (2).

In order to highlight the role of the Hund's coupling, we present calculations for $J = 0$, showing that two orbitals d_{xz} and d_{yz} remain equally filled and more occupied than the d_{xy} one, for all the values of U and no superconducting state is found, see Fig. 3 for $n = 3 + 1/3$. Therefore, it turns out that the symmetry breaking between d_{xz} and d_{yz} orbitals and superconductivity are intimately related (and their common origin requires a sizeable J/U).

We finally notice the role of the underlying band structure. Indeed, a simpler tight-binding Hamiltonian \mathcal{H}_0 with the same diagonal nearest-neighbor hopping for every orbital, displays superconductivity for $n = 3 + 1/3$, but with the $d_{x^2-y^2}$ symmetry [39], that one obtains for the one-band Hubbard model [46]. This finding underlies that, even in a model with only local electronic interactions, the symmetry of the order parameter depends on the shape of the Fermi surface.

Conclusions. By using variational wave functions including pairing parameters and Jastrow factors, we have studied a simplified model for IBS superconductors. Spanning the density range between $n = 3$ (Mott insulator) and $n = 4$ (Hund's metal), we find a nematic state with orbital-selective character and superconducting pairing. In particular, the d_{yz} (or d_{xz}) orbital remains half-filled in the whole density regime, thus leading to a spontaneous orbital-selective Mott transition and a broken rotational symmetry. Most importantly, superconductivity is observed in the nematic regime, changing

its character when the electron doping is varied. For $3 < n \lesssim 3.5$, the d_{xy} orbital sustains long-range electron pairing. Instead, for $3.5 \lesssim n < 4$, finite pairing correlations are observed in the d_{xz} (or d_{yz}) orbital, even though the BCS parameters are small in the superconducting orbital; in this unconventional case, electron pairing can be established only through the hybridization with the other orbitals. All these features are triggered by the presence of Hund's coupling, since neither orbital selectivity nor superconductivity are found for $J = 0$. The tentative phase diagram for $3 \leq n \leq 4$ is shown in Fig. 4.

Our work underlines how non-local correlations enrich the scenario of Hund's driven correlations with respect to DMFT, and establish a strong link between nematic correlations and superconductivity. The results are reminiscent of several observations in IBS, but we believe that a closer comparison with experiments must be deferred to future studies of more involved and complete models.

We acknowledge useful discussions with L. Fanfarillo. Computational resources were provided by HPC@POLITO (<http://www.hpc.polito.it>). We acknowledge also the CINECA award under the ISCRA initiative, for the availability of high performance computing resources and support. M.C. acknowledges financial support of MUR via PRIN 2020 (Prot. 2020JLZ52N 002) programs, and by the European Union - NextGenerationEU through PRIN 2022 (Prot. 20228YCY7), National Recovery and Resilience Plan (NRRP) MUR Project No. PE0000023-NQSTI, and No. CN00000013-ICSC. The views and opinions expressed are solely those of the authors and do not necessarily reflect those of the European Union, nor can the European Union be held responsible for them.

SUPPLEMENTAL MATERIAL

Three-orbital Hubbard model

The tight-binding Hamiltonian considered in this work is easily defined in momentum space as:

$$\mathcal{H}_0 = \sum_k \sum_{\alpha, \beta} \sum_{\sigma} c_{k, \alpha, \sigma}^{\dagger} T_{\alpha, \beta}(k) c_{k, \beta, \sigma}, \quad (3)$$

where α and β are orbital indices ($1 = xz$, $2 = yz$, and $3 = xy$), while $c_{k, \alpha, \sigma}^{\dagger}$ ($c_{k, \alpha, \sigma}$) is the fermionic operator that creates (annihilates) an electron in orbital α , with momentum k and spin σ . The intra- and inter-orbital

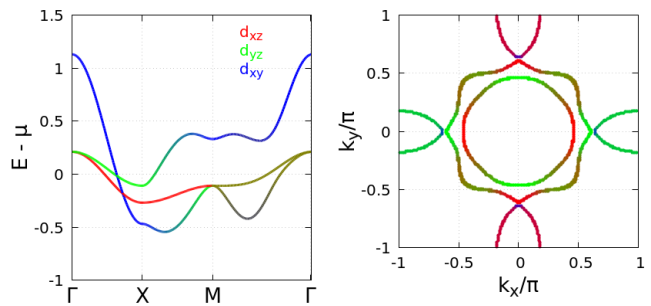


FIG. 5. Left panel: Band structure of the tight-binding model of Eqs. (3) along a selected path in the Brillouin zone, connecting the points $\Gamma = (0, 0)$, $X = (\pi, 0)$, and $M = (\pi, \pi)$; the chemical potential at density $n = 3 + 1/3$ is subtracted in order to have the Fermi energy at $E = 0$. The color code denotes the dominant orbital contribution to each band: d_{xz} (red), d_{yz} (green), and d_{xy} (blue). Right panel: Fermi surface for the electron density $n = 3 + 1/3$. The color code is the same as in the left panel.

hoppings are given as:

$$\begin{aligned} T_{1,1}(k) &= 2t_2 \cos k_x + 2t_1 \cos k_y + 4t_3 \cos k_x \cos k_y, \\ T_{2,2}(k) &= 2t_1 \cos k_x + 2t_2 \cos k_y + 4t_3 \cos k_x \cos k_y, \\ T_{3,3}(k) &= 2t_5 (\cos k_x + \cos k_y) + 4t_6 \cos k_x \cos k_y + \epsilon_{xy}, \\ T_{1,2} &= T_{2,1}^* = 4t_4 \sin k_x \sin k_y, \\ T_{1,3} &= T_{3,1}^* = 2it_7 \sin k_x + 4it_8 \sin k_x \cos k_y, \\ T_{2,3} &= T_{3,2}^* = 2it_7 \sin k_y + 4it_8 \sin k_y \cos k_x. \end{aligned}$$

In this work, we fix the hopping parameters (in units of eV): $t_1 = 0.02$, $t_2 = 0.06$, $t_3 = 0.03$, $t_4 = -0.01$, $t_5 = 0.1$, $t_6 = 0.15$, $t_7 = -0.1$, $t_8 = -t_7/2$ [27]. The orbital d_{xy} has a crystal field $\epsilon_{xy} = 0.2$ (notice that a slight different choice has been proposed in Ref. [34]). With the present choice of the hopping parameters, the total bandwidth is $W \approx 1.6\text{eV}$. The band structure and the corresponding Fermi surface are reported in Fig. 5 for density $n = 3 + 1/3$.

The interaction terms are defined by the Hubbard-Kanamori Hamiltonian:

$$\begin{aligned} \mathcal{H}_{\text{int}} &= U \sum_R \sum_{\alpha} n_{R, \alpha, \uparrow} n_{R, \alpha, \downarrow} \\ &+ U' \sum_R \sum_{\alpha \neq \beta} n_{R, \alpha, \uparrow} n_{R, \beta, \downarrow} \\ &+ (U' - J) \sum_R \sum_{\alpha > \beta} \sum_{\sigma} n_{R, \alpha, \sigma} n_{R, \beta, \sigma} \\ &- J \sum_R \sum_{\alpha \neq \beta} c_{R, \alpha, \uparrow}^{\dagger} c_{R, \alpha, \downarrow} c_{R, \beta, \downarrow}^{\dagger} c_{R, \beta, \uparrow} \\ &+ J \sum_R \sum_{\alpha \neq \beta} c_{R, \alpha, \uparrow}^{\dagger} c_{R, \alpha, \downarrow}^{\dagger} c_{R, \beta, \downarrow} c_{R, \beta, \uparrow}, \quad (4) \end{aligned}$$

where $n_{R, \alpha, \sigma} = c_{R, \alpha, \sigma}^{\dagger} c_{R, \alpha, \sigma}$ is the density operator on site R , orbital α and spin σ ; U and U' are the intra-

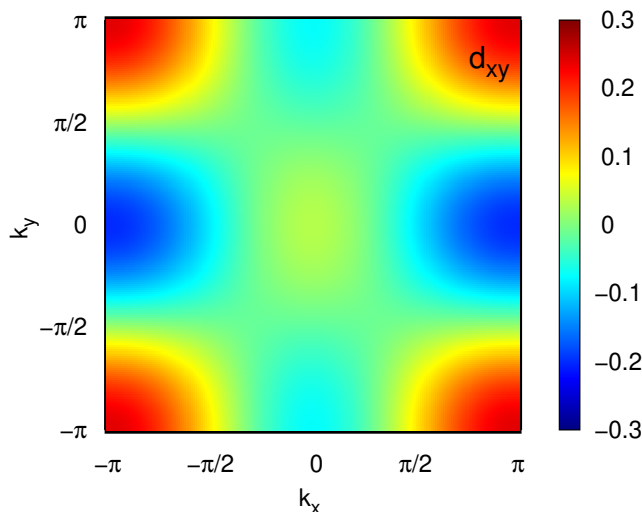


FIG. 6. Fourier transform $\Delta_{\alpha,k}$ for the d_{xy} orbital, computed for the optimal BCS parameters at density $n = 3 + 1/3$ in the orbital-selective regime at $U = 2\text{eV}$ and $J/U = 0.2$. Data are reported on the $L = 12 \times 12$ cluster.

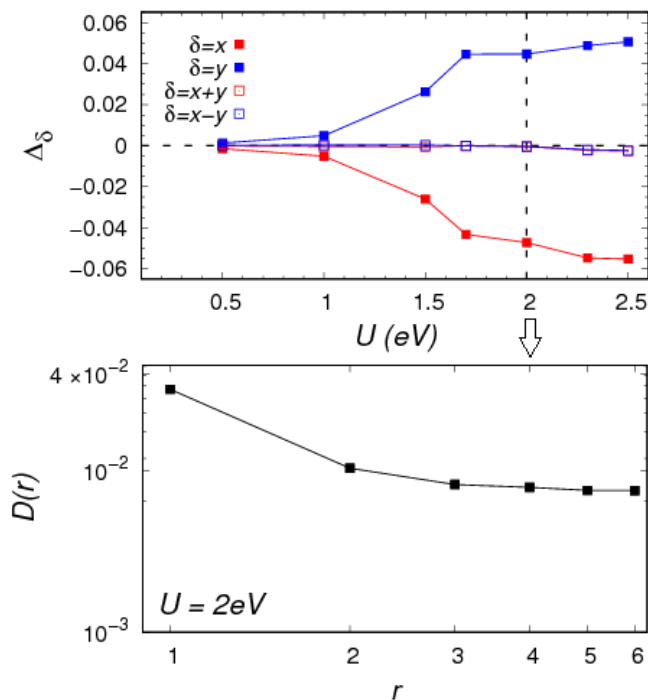


FIG. 7. Upper panel: Optimal intra-orbital BCS parameters (the same in each orbital), as a function of U for $n = 3 + 1/3$, when the tight-binding Hamiltonian contains only a nearest-neighbor hopping $t = -0.3\text{eV}$, see Eq. (6). Lower panel: Pairing-pairing correlations $D(r)$ [see Eq (7)] at $U = 2\text{eV}$, in the region where the optimal BCS parameters are finite. Results are obtained with the variational approach on a 12×12 cluster, for $J/U = 0.2$.

orbital and inter-orbital Hubbard interactions, respectively, and J is the Hund's coupling. We assume the system to be rotationally invariant, and thus $U' = U - 2J$ [17].

Fourier transform of the BCS parameters at density $n = 3 + 1/3$

The symmetry of the BCS parameters is highlighted in k -space, where:

$$\Delta_{\alpha,k} = 2[\Delta_{\alpha,x} \cos(k_x) + \Delta_{\alpha,y} \cos(k_y) + \Delta_{\alpha,x-y} \cos(k_x - k_y) + \Delta_{\alpha,x+y} \cos(k_x + k_y)]. \quad (5)$$

In particular, the results for the d_{xy} orbital (where superconductivity emerges at $n = 3 + 1/3$) are reported in Fig. 6, inside the nematic regime (for $U = 2\text{eV}$). Here, $\Delta_{xy,k}$ changes sign between the hole pocket around $\Gamma = (0, 0)$ and the electron pockets around the $X = (\pi, 0)$ and $Y = (0, \pi)$, resembling the s^\pm symmetry. The underlying broken symmetry induces a nematic BCS pairing in the d_{xy} orbital, with a clear difference between X and Y points. This feature derives from the fact that, in real space, the BCS parameters connecting nearest-neighbor sites are different, with $|\Delta_{xy,y}| > |\Delta_{xy,x}|$.

Results for the simplified multiorbital model

Here, we show the results for the simplified tight-binding model that is defined by considering only a nearest-neighbor intra-orbital hopping t , that is the same for the three orbitals. The hopping matrix in momentum space is then defined as:

$$T_{\alpha,\beta}(k) = 2t[\cos k_x + \cos k_y]\delta_{\alpha,\beta}. \quad (6)$$

We report in Fig. 7 the results for the pairing amplitudes Δ_δ and for the pairing-pairing correlations $D(r)$, defined as:

$$D(r) = \frac{1}{L} \sum_R \langle P_R P_{R+rx}^\dagger \rangle, \quad (7)$$

where $P_R = c_{R+y,\downarrow} c_{R,\uparrow} - c_{R+y,\uparrow} c_{R,\downarrow}$. In this case, the orbital index is dropped since the results are identical for all the orbitals.

Our results show that this model displays superconductivity for $n = 3 + 1/3$, but with the $d_{x^2-y^2}$ symmetry, that one obtains also for the one-band Hubbard model [46].

[1] Y. Kamihara, T. Watanabe, M. Hirano, and H. Hosono, *J. Am. Chem. Soc.* **130**, 3296 (2008).

- [2] R. M. Fernandes, A. I. Coldea, H. Ding, I. R. Fisher, P. J. Hirschfeld, and G. Kotliar, *Nature* **601**, 35 (2022).
- [3] K. Haule, J. H. Shim, and G. Kotliar, *Phys. Rev. Lett.* **100**, 226402 (2008).
- [4] I. I. Mazin, D. J. Singh, M. D. Johannes, and M. H. Du, *Phys. Rev. Lett.* **101**, 057003 (2008).
- [5] S. Raghu, X.-L. Qi, C.-X. Liu, D. J. Scalapino, and S.-C. Zhang, *Phys. Rev. B* **77**, 220503 (2008).
- [6] Q. Si and E. Abrahams, *Phys. Rev. Lett.* **101**, 076401 (2008).
- [7] F. Wang, H. Zhai, Y. Ran, A. Vishwanath, and D.-H. Lee, *Phys. Rev. Lett.* **102**, 047005 (2009).
- [8] A. Chubukov, *Annual Review of Condensed Matter Physics* **3**, 57 (2012).
- [9] R. M. Fernandes, A. V. Chubukov, and J. Schmalian, *Nature Physics* **10**, 97 (2014).
- [10] A. Chubukov, “Itinerant electron scenario,” in *Iron-Based Superconductivity*, edited by P. D. Johnson, G. Xu, and W.-G. Yin (Springer International Publishing, 2015) pp. 255–329.
- [11] A. V. Chubukov, M. Khodas, and R. M. Fernandes, *Phys. Rev. X* **6**, 041045 (2016).
- [12] D.-W. Yao and T. Li, *Journal of Physics: Condensed Matter* **30**, 495601 (2018).
- [13] A. Kreisel, B. M. Andersen, P. O. Sprau, A. Kostin, J. C. S. Davis, and P. J. Hirschfeld, *Phys. Rev. B* **95**, 174504 (2017).
- [14] H. Hu, R. Yu, E. M. Nica, J.-X. Zhu, and Q. Si, *Phys. Rev. B* **98**, 220503 (2018).
- [15] L. Benfatto, B. Valenzuela, and L. Fanfarillo, *npj Quantum Materials* **3**, 56 (2018).
- [16] Z. P. Yin, K. Haule, and G. Kotliar, *Nature Materials* **10**, 932 (2011).
- [17] A. Georges, L. de Medici, and J. Mravlje, *Annual Review of Condensed Matter Physics* **4**, 137 (2013).
- [18] L. de’ Medici, G. Giovannetti, and M. Capone, *Phys. Rev. Lett.* **112**, 177001 (2014).
- [19] P. O. Sprau, A. Kostin, A. Kreisel, A. E. Böhrer, V. Taufour, P. C. Canfield, S. Mukherjee, P. J. Hirschfeld, B. M. Andersen, and J. C. S. Davis, *Science* **357**, 75 (2017).
- [20] M. Yi, Z.-K. Liu, Y. Zhang, R. Yu, J.-X. Zhu, J. Lee, F. Moore, R. G. Schmitt, W. Li, S. Riggs, J.-H. Chu, B. Lv, J. Hu, M. Hashimoto, S.-K. Mo, Z. Hussain, Z. Mao, C. Chu, I. Fisher, Q. Si, Z.-X. Shen, and D. Lu, *Nat. Comm* **6**, 7777 (2015).
- [21] A. Kostin, P. O. Sprau, A. Kreisel, Y. X. Chong, A. E. Böhrer, P. C. Canfield, P. J. Hirschfeld, B. M. Andersen, and J. C. S. Davis, *Nature Materials* **17**, 869 (2018).
- [22] M. Capone, *Nature Materials* **17**, 851 (2018).
- [23] L. de’ Medici, *Phys. Rev. Lett.* **118**, 167003 (2017).
- [24] P. Villar Arribi and L. de’ Medici, *Phys. Rev. Lett.* **121**, 197001 (2018).
- [25] M. Chatzileftheriou, A. Kowalski, M. Berović, A. Amaricci, M. Capone, L. De Leo, G. Sangiovanni, and L. de’ Medici, *Phys. Rev. Lett.* **130**, 066401 (2023).
- [26] E. M. Nica, R. Yu, and Q. Si, *npj Quantum Materials* **2**, 24 (2017).
- [27] L. Fanfarillo, A. Valli, and M. Capone, *Phys. Rev. Lett.* **125**, 177001 (2020).
- [28] L. Fanfarillo, A. Valli, and M. Capone, *Phys. Rev. B* **107**, L081114 (2023).
- [29] M. Capone, M. Fabrizio, C. Castellani, and E. Tosatti, *Phys. Rev. Lett.* **93**, 047001 (2004).
- [30] M. Capone, M. Fabrizio, C. Castellani, and E. Tosatti, *Rev. Mod. Phys.* **81**, 943 (2009).
- [31] A. Georges, G. Kotliar, W. Krauth, and M. J. Rozenberg, *Rev. Mod. Phys.* **68**, 13 (1996).
- [32] L. de’ Medici and M. Capone (Springer International, 2017) pp. 115–185.
- [33] J. Kanamori, *Prog. Theor. Phys.* **30**, 275 (1963).
- [34] M. Daghofer, A. Nicholson, A. Moreo, and E. Dagotto, *Phys. Rev. B* **81**, 014511 (2010).
- [35] R. M. Fernandes and A. V. Chubukov, *Reports on Progress in Physics* **80**, 014503 (2016).
- [36] L. de’ Medici, S. R. Hassan, M. Capone, and X. Dai, *Phys. Rev. Lett.* **102**, 126401 (2009).
- [37] A. V. Chubukov, D. V. Efremov, and I. Eremin, *Phys. Rev. B* **78**, 134512 (2008).
- [38] K. Seo, B. A. Bernevig, and J. Hu, *Phys. Rev. Lett.* **101**, 206404 (2008).
- [39] “See supplemental material at...”.
- [40] F. Becca and S. Sorella, *Quantum Monte Carlo Approaches for Correlated Systems* (Cambridge University Press, 2017).
- [41] M. Capello, F. Becca, M. Fabrizio, S. Sorella, and E. Tosatti, *Phys. Rev. Lett.* **94**, 026406 (2005).
- [42] C. De Franco, L. F. Tocchio, and F. Becca, *Phys. Rev. B* **98**, 075117 (2018).
- [43] S. Sorella, *Phys. Rev. B* **71**, 241103 (2005).
- [44] T. Misawa and M. Imada, *Nature Communications* **5**, 5738 (2014).
- [45] A. Amaricci, L. Crippa, A. Scazzola, F. Petocchi, G. Mazza, L. de Medici, and M. Capone, *Computer Physics Communications* **273**, 108261 (2022).
- [46] L. F. Tocchio, F. Becca, and S. Sorella, *Phys. Rev. B* **94**, 195126 (2016).